University of Barcelona

Master in Quantum Science and Technology

MASTER'S THESIS

ENERGY STORAGE AND QUANTUM SIMULATIONS WITH OPTICAL NETWORKS

UNIVERSITAT DE BARCELONA

ICFO

Beatriz Polo Rodríguez

Supervisors: Federico Centrone, Paolo Stornati, Antonio Acín

Course 2023-2024

Energy storage and quantum simulations with optical networks

Beatriz Polo

Supervised by: Federico Centrone, Paolo Stornati, Antonio Acín

Instituto de Ciencias Fotónicas, 08860 Castelldefels (Barcelona)

June 2024

Quantum optical neural networks (QONN) stand out as promising variational algorithms for quantum simulations by leveraging the potential advantages of photonic circuits with respect to other hardware platforms. In this work, the basics of our proposed physically-inspired architecture of a continuous-variable QONN and its applicability to both optimization of quantum energy storage devices and simulation of quantum field theory will be discussed. Concerning the former, the dependence of the relative energy precision on stellar rank and bipartite correlations in quantum battery systems will be analysed, whereas for the latter, a preliminary study of the Orbifold formulation of U(1) Yang-Mills theory through exact diagonalisation will be presented.

Keywords: Photonic circuits, Gaussian states, covariance matrix, non-gaussianity, stellar rank, single-photon operations, batteries, signal-to-noise ratio, lattice regularization, Orbifold construction, gauge symmetry.

Beatriz Polo: beatriz.polo@icfo.eu

Acknowledgements

This work would have never been possible without the dedication and mentoring of my thesis supervisors, Fede and Paolo. Thank you for sharing your knowledge and expertise, for your contagious passion for quantum physics, for your help and patience, and for fun and enriching discussions. You are the best people I could have asked for to guide the first steps into my research career.

I would also like to extend my gratitude to Toni, for offering me the opportunity to become a member of his Quantum Information Theory group and undertake this experience in such an exceptional scientific environment. To the rest of QIT members, I am truly grateful for your warm welcome, friendly advice, and for making ICFO feel like home. Special thanks to three inspiring women that I have come across this year. Júlia, Mariana and Egle, you are amazing.

To my fellow classmates and friends, both from the bachelor's and from the master. These years of both personal and academic growth would not have been the same without you. Clara, Ángela, Laura, Alejandro, Pablo. I appreciate and admire each of you.

A huge thanks goes to my family, Miquel, and all the rest of my friends, who have given me the encouragement, love and support needed to pursue my goals, and without whom none of this would have been achievable. I could not be luckier to have you by my side.

Contents

1 Introduction

1.1 Quantum Optical Networks

One of the most prominent motivations for quantum computing research is predicting the properties and dynamics of complex quantum systems. Simulating their non-classical features using classical methods appears increasingly impractical due to the exponential growth in complexity [Fey81]. Consequently, there is a growing interest in developing quantum simulation algorithms that are physically motivated and tailored to leverage specific near-term quantum hardware [SOEC18]. Among various proposals, Quantum Optical Neural Networks (QONNs) stand out as a type of variational algorithm able to efficiently perform a range of quantum information processing tasks, including quantum simulations, by relying on the unique properties of light particles as information carriers in photonic hardware [OFV09].

Experiments involving light are at the heart of our understanding of the complex implications of the laws of quantum mechanics, with the entanglement of photon pairs, for example, as a historically crucial piece of evidence in support of quantum mechanics over hidden variable theories [ADR82]. Photons do not naturally interact with each other easily, constituting a robust system that is inherently free from decoherence. In addition, photons can be manipulated and individually addressed at room temperature with a high degree of experimental control using various components, including passive optics, non-linear crystals, single-photon detectors, and homodyne detectors [CHK+20] [AGW12]. They can be transported in free space or through waveguides, allowing interaction beyond nearest neighbors and high-speed transmission of information. Notably, many of the building blocks of neural networks in machine learning have a very natural mapping into the quantum optical domain [KBA+19], with beam splitters, programmable phase shifters, and optical nonlinearity playing the analog roles to weights, biases, and activation functions in network layers, respectively. These properties, along with the rapid development of photonic quantum technologies have resulted in some quantum advantage experiments already being conducted using photonic systems, making them a logical choice and a leading approach to quantum information processing [ZWD+20],[MLA+22].

1.2 Continuous Variables Quantum Information

The Continuous Variable (CV) framework is characterized by the encoding of quantum information in observables that span continuous ranges of values, such as position and momentum, or analogously amplitude and phase. The standard approach to quantising the motional degrees of freedom of a bosonic non-relativistic particle consists in defining a pair of self-adjoint 'canonical' operators $\hat{x}$, $\hat{p}$, known as quadratures, that satisfy the so-called canonical commutation relation (CCR):

$$[\hat{x}, \hat{p}] = i\hat{\mathbb{1}} \tag{1}$$

in which we have assumed natural units, where $\hbar = 1$. These quadrature operators represent the position and momentum of the particle in the quantum harmonic oscillator description, with continuous spectra covering the whole real line. If more than one degree of freedom or *mode* is considered, one can generalize the CCR above by defining a vector of canonical operators $\hat{\mathbf{s}} = (\hat{x}_1, \dots \hat{x}_N, \hat{p}_1, \dots \hat{p}_N)^T$ such that:

$$[\hat{\mathbf{s}}, \hat{\mathbf{s}}^T] = iJ, \text{ with } J = \begin{pmatrix} 0_N & \mathbb{1}_N \\ -\mathbb{1}_N & 0_N \end{pmatrix} \quad \text{equivalent to } [\hat{x}_j, \hat{p}_k] = i\delta_{jk} \tag{2}$$

The commutation relation in Eq.1 may be equivalently expressed in terms of the non-hermitian bosonic ladder operators, which in this same harmonic oscillator picture account for the creation or destruction of a quantum of energy.

$$\left.\begin{aligned} \hat{a}_j &= \frac{1}{\sqrt{2}}(\hat{x}_j + i\hat{p}_j) \\ \hat{a}_k^\dagger &= \frac{1}{\sqrt{2}}(\hat{x}_k - i\hat{p}_k) \end{aligned}\right\} \Longrightarrow [\hat{a}_j, \hat{a}_k^\dagger] = \delta_{jk} \tag{3}$$

In quantum field theory, where relativistic systems with varying number of particles are considered through the formalism of second quantization, the action of these two operators describes the creation and destruction of particles, while $\hat{x}$, $\hat{p}$ stand for a pair of bosonic field operators (like the electric and magnetic components of the electromagnetic field, for example).

It can be shown that the algebra defined by the canonical commutation relations (Eq.1) does not allow for a representation through finite dimensional matrices, not even when a finite number of degrees of freedom are considered [Ser21]. The particularly complex information and correlation properties of systems that require Hilbert spaces of infinite dimension lead to a dichotomy between the 'easily tractable' subset of continuous variable states and those that lie out of this realm. The next two sections discuss these two categories, known as Gaussian and non-gaussian, respectively.

1.2.1 Gaussian states. Covariance matrix formalism

Gaussian states are a central object of study within continuous-variable quantum information despite comprising a very reduced fraction of the whole Hilbert space. They are the ones involved in most experimental processes, owing to their manipulability with current technology. Any Gaussian state ρ_G can be written as:

$$\rho_G = \frac{e^{-\hat{H}/k_B T}}{\mathrm{Tr}(e^{-\hat{H}/k_B T})} \tag{4}$$

where T is the temperature of the system and k_B is the Boltzmann constant, corresponding the limit $T \to 0$ to pure states. $\hat{H}$ is any bounded-from-below Hamiltonian, at most quadratic in the quadrature variables. The restriction to Gaussian probability distributions in phase space notably simplifies the mathematical treatment of Gaussian states. It implies that they can be fully characterized by their vector of first moments $\bar{\mathbf{r}}$ and their covariance matrix σ, which are in practice accessible as the first and second statistical moments, respectively, of measurements of the canonical operators. First moments contain information that is relevant in the context of quantum communication or metrology, but since they can be arbitrarily adjusted by unitary displacement operators, they do not play any role in properties regarding entropy or entanglement, which are invariant under local unitary operations. Hence they are often set to zero and neglected in literature [CC22], as will be the case in our analysis. We will thus proceed by focusing solely on the covariance matrices (CM), which, with regard to the previous considerations, uniquely characterize Gaussian states.

Through the normal decomposition or Williamson's theorem first proposed in [Wil36],

one can express the covariance matrix[1] of the most general N-mode Gaussian state as:

$$\sigma = S\left(\bigoplus_{j=1}^{N} \nu_j \mathbb{1}_2\right) S^T \tag{6}$$

where $S \in Sp_{2n,\mathbb{R}}$ is a generic symplectic matrix and the $\nu_j \geq 1$ are referred to as the symplectic eigenvalues, related to the temperature of the system and the frequency of each of the normal modes through the expression:

$$\nu_j(\gamma_j) = 1 + \frac{2}{e^{1/\gamma_j} - 1} \tag{7}$$

where we have defined the dimensionless parameter

$$\gamma_j \equiv \frac{k_B T}{\omega_j} \tag{8}$$

The symplectic matrix S embeds all possible Gaussian transformations (i.e. operations that map Gaussian states to Gaussian states, and which are by definition generated by at most second-order Hamiltonians in $\hat{x}, \hat{p}$) that can act on a state, disregarding linear displacements which leave the covariance matrix unchanged and affect the first moments vector only. Among a series of possible decompositions of symplectic transformations, the Bloch-Messiah or singular value decomposition [BM62] appears to be especially useful to our purposes due to its physical interpretability:

$$S = O_1 Z O_2 \qquad \forall S \in Sp_{2n,\mathbb{R}} \tag{9}$$

$$\text{with} \quad O_1, O_2 \in O(2N) \cap Sp_{2n,\mathbb{R}} \cong U(N) \quad \text{and} \quad Z = \bigoplus_{j=1}^{N} \begin{pmatrix} z_j & 0 \\ 0 & z_j^{-1} \end{pmatrix}$$

The transformations O_1, O_2 are energy-preserving or *passive optics* transformations, each of them comprising beam splitters (semi-reflective mirrors parametrised by their transmissivity $cos(\theta)^2$ that mix up two modes) and phase shifters (dielectric plates that rotate the optical phase of an electromagnetic wave by some angle φ). A scheme of alternating applications of these two operations to create the most general linear interferometer is detailed in [TR19]. Matrix Z represents local or single-mode squeezing, which in contrast, is an active operation, requiring energy from an external laser field that pumps a nonlinear crystal through which the optical modes travel, and also injecting energy into the system. The result of this transformation is a contraction of the variance of one of the canonical variables and the expansion of that of its conjugate one, and an output state with the potential of acquiring correlations among the different modes once mixed in the beam splitter.

[1] Independently of such factorization, there exists a geometric necessary and sufficient condition, known as the Robertson-Schrödinger uncertainty relation, for a symmetric matrix to represent the covariances of a quantum state, namely:

$$\sigma + i\Omega \geq 0 \quad \text{with } \Omega = \bigoplus_{j=1}^{N} \begin{pmatrix} 0 & 1 \\ -1 & 0 \end{pmatrix} \tag{5}$$

which is in fact equivalent to the condition $\nu_j \geq 1 \ \forall j \in \{1 \dots N\}$ on the symplectic eigenvalues. It is also worth noting, for completeness, that a Gaussian state is pure if and only if its covariance matrix has determinant 1, if and only if all its symplectic eigenvalues are equal to 1.

The parametrization of covariance matrices given in Eqs.6-9 allows for an alternative definition of Gaussian states in terms of the just defined universal set of Gaussian transformations. According to the Bloch-Messiah prescription, a Gaussian state of N modes is then described as any state that can be obtained by applying a product of N single-mode squeezers, N phase shifters and $\frac{N(N-1)}{2}$ two-mode beam splitters on the vacuum state $\bigotimes_{j=1}^{N} |0\rangle_j$, after thermalisation with a reservoir at temperature T.

1.2.2 Non-gaussian continuous variable states

As explained above, the restriction to Gaussian states fails to exhaust most of the continuous-variables Hilbert space, which, in the context of variational algorithms, makes an ansatz so little expressive that the possibility to find the optimum within the explored subset barely exists. From a more fundamental point of view, the statistics of Gaussian states can be reproduced by classical distributions, so no real quantum effects can be observed with this limitation. Instead, non-gaussianity must be considered to exploit quantum non-locality and observe computational supremacy.

The possibilities for our non-gaussian ansatz are infinite, however, we have chosen to focus on a particular, iteratively-constructed form of states, namely those built from consecutive photon additions or subtractions[2] [3] on a previously Gaussian state.

$$\rho_{NG} = \begin{cases} (\hat{a}_1^\dagger)^m U_G \rho_0 U_G^\dagger (\hat{a}_1)^m & \text{for additions} \\ (\hat{a}_1)^m U_G \rho_0 U_G^\dagger (\hat{a}_1^\dagger)^m & \text{for subtractions} \end{cases} \quad m = 1, 2 \dots \tag{10}$$

Several aspects contribute to motivating this choice. First, adding or subtracting a single photon from the radiation field is the most fundamental process by which matter interacts with light, and thus the most straightforward way in which novel non-classical states of light have so far been experimentally produced. Although the effective preparation of photon added and subtracted states on readily available quantum hardware [BJML10][NNNH$^+$06] is technically challenging and only achievable in a stochastic fashion, with vanishing success probability as the number of single-photon operations m increases, it is still interesting to study this protocols at least theoretically, due to the valuable insights they provide on the behaviour of quantum correlations in light modes.

On the one hand, because the form of photon added and subtracted states constitutes an approach to universality, owing to the fact that any continuous variable state can be approximated by a polynomial in the ladder operators applied to a Gaussian state. On the other hand, by inspection of Equation 10, one realizes that photon-additions, when the Gaussian operation U_G is the identity, yield nothing but the Fock basis; so by means of tuning the Gaussian parameters, these states offer an interpolation between the discrete and continuous variables realms.

Precisely due to the probabilistic nature of photon subtraction and addition, the statistics of states yielding from these processes exhibit some counter-intuitive and interesting properties [BFGS18]. As a most prominent example, there is the fact that the mean photon number for an initial thermal state can be increased by subtracting photons from it, which

[2] A schematic description of how these operations are experimentally performed is given in Appendix D

[3] Note that all photon additions/ subtractions act on the first mode without loss of generality, since swapping two modes is a Gaussian operation[CFGM21].

would be impossible due to photon-number conservation if the procedure was deterministic. Many of these properties, which we seek to prove are resources for energy processing matters, are highly influenced by the nature of the initial photon-number distribution, and by whether it undergoes photon antibunching, an inherently quantum process described in Appendix C.

Quantifying non-gaussianity of an arbitrary state is typically carried out through the so-called *stellar rank*, a parameter that counts the amount of zeros in the state's Husimi Q-characteristic function. This approach to assessing non-gaussianity is in general computationally complex, however, when it comes to states engineered through consecutive single-photon operations, like the ones we are restricting ourselves to, it can be proven [CM22] that a non-gaussian state, either pure or mixed, has stellar rank n if at least n photon subtractions or additions are needed to prepare this state from the vacuum. This criterion will be key to grounding our conclusions in the coming sections.

1.2.3 Entanglement in CV states

Most well-known entanglement criteria (PPT, Giedke-Cirac, logarithmic negativity) are based on second moments, can thus be fully computed upon knowledge of the covariance matrix and establish necessary and sufficient conditions for a Gaussian state to be entangled. Outside the Gaussian domain, states are no longer fully described by accessing first and second-order moments only, due to the higher complexity of their correlations. The above-mentioned criteria can still be applied, but for non-gaussian states one can only aspire to obtain entanglement witnesses out of them, rather than *if and only if* conditions. However, in [SV05] a more powerful inequality was proposed, able to detect continuous-variable bipartite entanglement of generic states[4] by involving higher-order statistical moments of the quadrature operators. Below we provide the two-mode version of the theorem for the sake of simplicity:

Theorem 1 (SV Criterion for entanglement)**.** *Let $\hat{a}$ and $\hat{b}$ be the annihilation operators for modes A and B, respectively. Then, the negativity of the determinant of any of the principal submatrices of matrix M (see Eq.11) is a sufficient condition for the non-positivity of the partial transposition of a two-mode bipartite state, and hence for its entanglement.*

$$\mathrm{M}=\begin{pmatrix} 1 & \langle\hat{a}\rangle & \langle\hat{a}^\dagger\rangle & \langle\hat{b}^\dagger\rangle & \langle\hat{b}\rangle & \langle\hat{a}\hat{a}^\dagger\rangle & \langle\hat{a}\hat{b}^\dagger\rangle & \cdots \\ \langle\hat{a}^\dagger\rangle & \langle\hat{a}^\dagger\hat{a}\rangle & \langle\hat{a}^{\dagger 2}\rangle & \langle\hat{a}^\dagger\hat{b}^\dagger\rangle & \langle\hat{a}^\dagger\hat{b}\rangle & \langle\hat{a}^\dagger\hat{a}\hat{a}^\dagger\rangle & \langle\hat{a}^\dagger\hat{a}\hat{b}^\dagger\rangle & \cdots \\ \langle\hat{a}\rangle & \langle\hat{a}^2\rangle & \langle\hat{a}\hat{a}^\dagger\rangle & \langle\hat{a}\hat{b}^\dagger\rangle & \langle\hat{a}\hat{b}\rangle & \langle\hat{a}^2\hat{a}^\dagger\rangle & \langle\hat{a}^2\hat{b}^\dagger\rangle & \cdots \\ \langle\hat{b}\rangle & \langle\hat{a}\hat{b}\rangle & \langle\hat{a}^\dagger\hat{b}\rangle & \langle\hat{b}^\dagger\hat{b}\rangle & \langle\hat{b}^2\rangle & \langle\hat{a}\hat{a}^\dagger\hat{b}\rangle & \langle\hat{a}\hat{b}^\dagger\hat{b}\rangle & \cdots \\ \langle\hat{b}^\dagger\rangle & \langle\hat{a}\hat{b}^\dagger\rangle & \langle\hat{a}^\dagger\hat{b}^\dagger\rangle & \langle\hat{b}^{\dagger 2}\rangle & \langle\hat{b}\hat{b}^\dagger\rangle & \langle\hat{a}\hat{a}^\dagger\hat{b}^\dagger\rangle & \langle\hat{a}\hat{b}^{\dagger 2}\rangle & \cdots \\ \langle\hat{a}\hat{a}^\dagger\rangle & \langle\hat{a}\hat{a}^\dagger\hat{a}\rangle & \langle\hat{a}\hat{a}^{\dagger 2}\rangle & \langle\hat{a}\hat{a}^\dagger\hat{b}^\dagger\rangle & \langle\hat{a}\hat{a}^\dagger\hat{b}\rangle & \langle\hat{a}\hat{a}^\dagger\hat{a}\hat{a}^\dagger\rangle & \langle\hat{a}\hat{a}^\dagger\hat{b}^\dagger\rangle & \cdots \\ \langle\hat{a}^\dagger\hat{b}\rangle & \langle\hat{a}^\dagger\hat{a}\hat{b}\rangle & \langle\hat{a}^\dagger\hat{b}\rangle & \langle\hat{a}^\dagger\hat{b}^\dagger\hat{b}\rangle & \langle\hat{a}^\dagger\hat{b}^2\rangle & \langle\hat{a}^\dagger\hat{a}\hat{a}^\dagger\hat{b}\rangle & \langle\hat{a}^\dagger\hat{a}\hat{b}^\dagger\hat{b}\rangle & \cdots \\ \vdots & \vdots & \vdots & \vdots & \vdots & \vdots & \vdots & \ddots \end{pmatrix} \tag{11}$$

The matrix is infinite-dimensional, as one can unboundedly consider higher orders in the quadrature operators. However, identifying one single negative principal minor is enough to certify that the state is entangled. In fact, for the states that concern us (up to three

[4] It must be taken into account that, although irrelevant and non-exploitable for information processing, communication and computation, this criterion is able to qualify distillable but not bound entanglement.

single-photon operations), it will be shown that it is sufficient to test the minor given by rows and columns 2 and 4 of matrix M, so our simplified version of the SV criterion reads:

$$SV = \langle \hat{a}^\dagger \hat{a} \rangle \langle \hat{b}^\dagger \hat{b} \rangle - \langle \hat{a}^\dagger \hat{b}^\dagger \rangle \langle \hat{a} \hat{b} \rangle < 0 \Longrightarrow \text{ entangled} \tag{12}$$

1.3 CV QONN architecture

In our quantum-optical approach to implementing a continuous-variable variational algorithm, each mode of the electromagnetic field is modeled as a quantum harmonic oscillator with its associated creation and annihilation operators and its canonically conjugate pair of quadrature variables playing the role of position and momentum observables. Our optimization routines recover the algorithm architecture proposed in [SAC+24], a schematic diagram of which is displayed in Fig.1 for clarification.

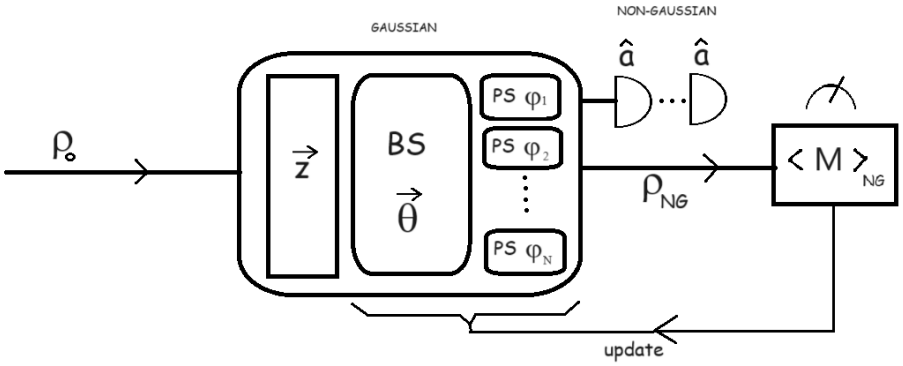

Figure 1: One-layer structure of our Quantum Optical Neural Network proposal

- The input of the quantum neural network is the N-mode (thermal) vacuum state, encoded in its covariance matrix.
- This initial state undergoes squeezing through nonlinear crystals and interference through a set of linear passive optics gates (beam splitters and phase shifters). This Gaussian block is parametrized by the vectors $\vec{z}, \vec{\theta}$, and $\vec{\varphi}$, randomly initialized.
- The introduction of non-gaussianity is accomplished by successive photon subtractions or additions on one of the modes. As commented before, the probability of success of these non-gaussianity creation methods is very low, in account for the preservation of fidelity of the resulting non-gaussian states, meaning that in the post-selected runs of detector clicks, we may assume we have a perfect photon added or subtracted state.
- Conditioned on successful subtraction or addition (that is, discarding all no-click events), the expectation value of our observable of interest (which acts as the cost function of the algorithm) is computed through homodyne measurements of field quadratures.
- Lastly, a classical gradient-descent-based optimizer is used to perform an update of the variational parameters of the Gaussian operations until the cost function reaches

an extremum value (either maximum or minimum, depending on the specific problem). The final vector of parameters comprises a complete description of the optimal state.

The manipulation of photon-added and subtracted states, both in terms of implementation and in theory, is far from trivial. However, throughout the execution of the algorithm, all we require is the computation of expectation values of interest[5] on our non-gaussian states:

$$\langle \hat{M} \rangle_{\hat{\rho}_{NG}} = \mathrm{Tr}\left[\hat{M}\hat{\rho}_{NG}\right].$$

which can be accomplished on account of Isserlis' theorem [ISS18], by simply accessing the entries of the covariance matrix of the Gaussian state prior to single-photon addition or subtraction. The calculation of these expectation values is explained in appendix A.

Once its structure has been formulated, this neural network can be applied to ground-state finding in many different scenarios, by simply adequately defining the observable to optimize, and the number of modes needed to represent the available degrees of freedom in the system. In the following sections, we will exploit its versatility in such diverse contexts as quantum thermodynamics and quantum field theory.

2 Quantum batteries

2.1 Motivation and basic concepts

The investigation of quantum batteries (QB) is crucial in the realm of quantum thermodynamics and quantum information science. Quantum batteries are devices that store and deliver energy by exploiting the unique properties of quantum mechanical systems, thus offering a novel approach to energy processing and manipulation that could potentially give a significant advantage in charging and storage performance and open new avenues for practical applications in various fields, from nano-scale devices to large-scale quantum networks. Moreover, as quantum technologies continue to advance and integrate into various applications, from quantum computing to quantum communication, the efficient storage and management of energy within these systems become increasingly essential.

A QB is defined as a system whose internal (or bare) Hamiltonian H_0 has non-degenerate energy levels[6], such that energy can be temporarily stored by performing unitary operations U on an initial state (assumed to be the groundstate ρ_0) in order to prepare the system in some excited state $\rho = U\rho_0 U^\dagger$. The stored, and later extractable energy from this process (known as ergotropy) is measured with respect to the internal Hamiltonian:

$$E_{extr} = E - E_0 = \mathrm{Tr}(H_0\rho) - \mathrm{Tr}(H_0\rho_0) \tag{13}$$

Most literature regarding this topic focuses on optimizing battery performance in terms of measures like charging power, charging times or energy storage capacity [FCA+18][CGQ+23].

[5]The analytical tools at hand impose the restriction that these observables be products of ladder operators. However, we encounter this as not such a restrictive condition because any quantum observable can be approximated by a polynomial in the ladder operations [HJ19]

[6]In fact, a more relaxed condition of a partially degenerated spectrum, i.e. such that the eigenvalues satisfy the relation $\epsilon_k \leq \epsilon_{k+1}$ as long as the bandwidth $\epsilon_{máx} - \epsilon_{min}$ is non-zero, is sufficient for the definition of a quantum battery.

However, little attention has been so far given to precision, a parameter that has a strong relationship with the intrinsic properties of quantum systems and at which these are far more likely to provide useful advantage over classical ones. Minimizing the uncertainty in the amount of energy accumulated in a quantum battery has promising applications in nanotechnology or other accuracy-related tasks. Hence the figure of merit that we will seek to maximize in this work is the inverse relative error in the extractable energy of the system, an adimensional quantity which we will refer to as extractable signal-to-noise ratio (SNR_{extr}):

$$SNR_{extr} = \frac{E_{extr}}{\Delta E} = \frac{E - E_0}{\Delta E} = \frac{E - E_0}{\sqrt{\langle E^2 \rangle - \langle E \rangle^2}} \tag{14}$$

Actually, this metric is closely related to the second-order correlation function $g^{(2)}(0)$, which characterizes photon antibunching and makes a powerful distinction between classical and non-classical light. The analytical link between this celebrated parameter and our signal-to-noise ratio is derived in Appendix C.

In the context of CV quantum information, the batteries we consider are infinite-dimensional bosonic systems of N modes, i.e. collections of N coupled harmonic oscillators, which are assumed to all have unit frequency $\omega_i = \omega = 1 \; \forall i \in \{1, \dots N\}$ and to be initially thermalized at some ambient temperature T. The Hamiltonian of this system is

$$\hat{H}_0 = \sum_{n=1}^{N} \left(\hat{a}_n^\dagger \hat{a}_n + \frac{1}{2} \right) = \sum_{n=1}^{N} \left(\hat{N}_n + \frac{1}{2} \right) \tag{15}$$

although the zero-point energy constant $\frac{N}{2}$ can be omitted in calculations since removing it yields the exact same operator's spectrum, it cancels when taking the difference in Eq.13 and as an additive constant, it does not influence the variance.

Our input state will be the tensor product of N single-mode thermal states:

$$\rho_0 = \bigotimes_{n=1}^{N} \tau_n(\gamma) \quad \text{where} \quad \tau_n(\gamma) = \frac{e^{-\hat{H}_0/\gamma}}{\mathrm{Tr}(e^{-\hat{H}_0/\gamma})} \tag{16}$$

These initial Gaussian states are the lowest energy eigenstates of the bare Hamiltonian at the fixed temperature T, and coincide with the N-mode vacuum $|0\rangle^{\otimes N}$ in the limit $T \to 0$ (which corresponds to $\gamma = 0$ by the definition in Eq. 8). Once defined the input states, and given that our chosen figure of merit (see Eq.14) is constructed from expectation values of observables which consist of products of ladder operators, we have arrived at a suitable formulation of the problem for the application of our CV QONN.

We seek to maximize SNR_{extr} over the continuous variable states that we can generate through our universal set of Gaussian operations, plus consecutive single photon subtractions and additions. Among the non-gaussian states, Fock states are optimal at null temperature, since they have a well-defined energy ($\Delta E = 0$). However, at fluctuation levels that are more realistic for implementations, this is no longer true, and there is in fact a critical temperature T_c above which finding the optimum becomes a non-trivial task, since Fock states not only lose optimality but turn to be the worst in terms of SNR_{extr}. Our approach to show the existence of such T_c can be found in appendix B. It is in this noisy regime in which experiments are normally conducted that we are interested in performing our optimization analysis. In what follows, we will restrict ourselves for simplicity to the two-mode ($N = 2$) case, and for the squeezing operation we will consider the second

mode always anti-squeezed ($\frac{1}{z}$) with respect to the first one (z), although the results can be generalised to arbitrary N and free squeezing parameters in a straightforward manner.

2.2 Results

2.2.1 Gaussian battery charging

First we study the phenomenon of battery charging through the application of Gaussian unitaries only. The analytical expression for the extractable signal-to-noise ratio after squeezing, beam splitting, and phase shifters turns out to be:

$$SNR_{extr}(\nu, z) = \nu \frac{z^2 - 2z + 1}{\sqrt{\nu^2 z^4 + \nu^2 - 2z^2}} \tag{17}$$

which is expressed in terms of the symplectic eigenvalue ν, uniquely mapped to γ through Eq.7, and only dependent on temperature once the assumption of homogeneous unit frequency has been fixed (see Eq.8). The dependence on the squeezing parameter for various noise levels $\gamma \in [0, 1.4]$ is shown below.

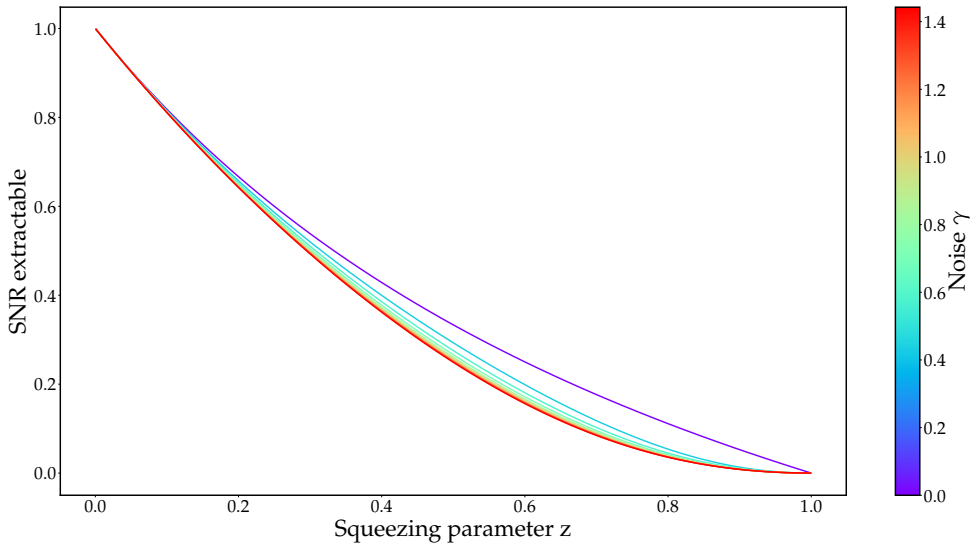

Figure 2: SNR_{extr} as a function of the squeezing parameter for several thermal fluctuation levels

Ratio values decrease as the setup becomes more noisy, being pure states ($T = 0K$) the optimal case. Nevertheless, from Eq.17 we encounter a strong limitation of Gaussian battery charging: its dependence solely on ν, z means that given a fixed temperature of the system, the only source of performance improvement is by means of varying the squeezing parameter. However, squeezing is an active process that can change the energy of the quantum states involved. This makes the system more complex to analyze and control, especially in terms of managing energy flow and avoiding unwanted energy injection or loss. Ideally, we would like to be able to charge our quantum states through passive optics operations, which are linear, energy-preserving maps applied through stable and little technically demanding optical elements. The fact that these operations do not yield any gains (i.e. the SNR_{extr} function is constant with respect to their parameters) motivates us to explore continuous variable states out of the Gaussian realm.

2.2.2 Non-gaussianity

Our next object of analysis is the performance of states to which, after the Gaussian block, consecutive single photon operations are applied. Figures 3 and 4 show the numerical results of extractable signal-to-noise energy ratio as a function of z obtained with the QONN, for increasing number of single-photon operations (additions and subtractions, respectively). The temperature for the simulations has been fixed at $\gamma = 0.5$.

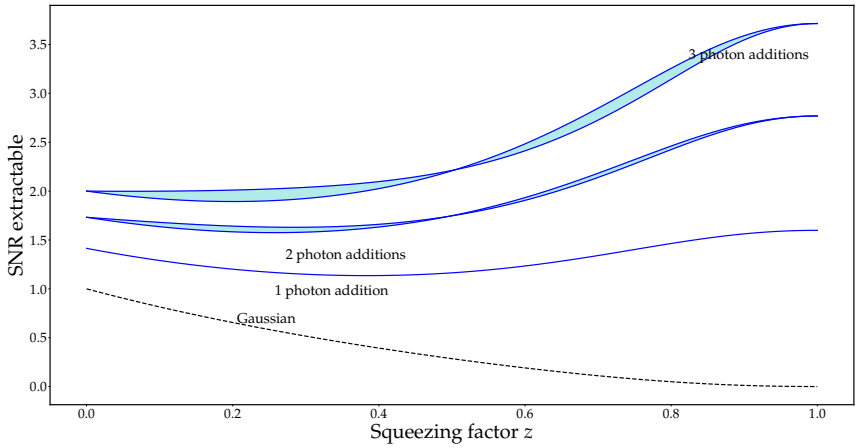

Figure 3: Bounds on SNR_{ext} for increasing amounts of photon additions as a function of z

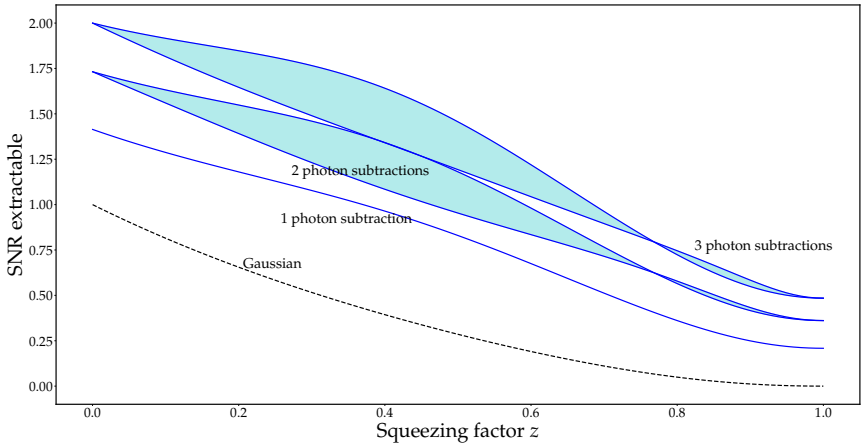

Figure 4: Bounds on SNR_{ext} for increasing amounts of photon subtractions as a function of z

The predominance of non-gaussian states over Gaussian ones in the context of energy processing had already been stated in previous references [FH18] [SAC+24]. Through simple set theory reasoning, one can conclude that for any function of interest $\mathcal{F}$, and in particular for SNR_{extr}:

$$\max_{U_G \in \mathcal{G}(\mathcal{U})} \mathcal{F}(U_G \rho_0 U_G^\dagger) \leq \max_{U \in \mathcal{U}} \mathcal{F}(U \rho_0 U^\dagger) \tag{18}$$

since the set of Gaussian unitaries is a subset of all possible unitaries $\mathcal{G}(\mathcal{U}) \subset \mathcal{U}$. However, here we show that the inequality in Eq.18 is in fact strict, and propose a concrete

iterative construction of non-gaussian states which has a feasible physical realization, and that establishes a hierarchy by which the bound on SNR_{extr} imposed by the restriction to gaussian states is violated by a greater amount as the stellar rank of our states (i.e. the number of single-photon operations required to engineer them [CM22]) increases.

Another feature worth noting is that, for the Gaussian and $m = 1$ cases, the plot displays a single SNR_{extr} curve, while for higher orders in the ladder operators, there is an area delimited by worst and best case scenarios. The reason for this is that the extractable signal-to-noise ratios for one single-photon operation still display no analytical dependence on $\theta, \phi_1,$ or ϕ_2. This implies that neither Gaussian nor single-photon added or subtracted states admit charging precision enhancement through passive optics. However, from two single-photon operations onwards, we do observe a periodic behaviour as a function of the angle of the beam splitter. It seems reasonable to interpret this effect as a result of the correlations that are created by the introduction of higher degrees of non-gaussianity into the system, and conjecture that there could exist a tight relationship between bipartite entanglement and SNR_{extr} of our states, by means of which the former is a direct resource for the latter. To test this hypothesis, we employ the SV criterion as a measure of bipartite entanglement, and plot both quantities as a function of the angle θ of the BS, for different squeezing values.

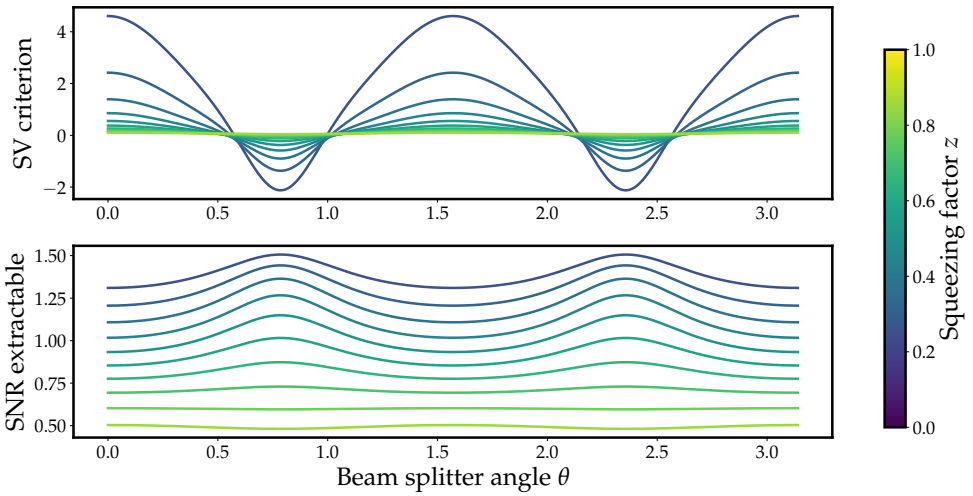

Figure 5: Periodic dependence of entanglement and SNR_{extr} on the beam splitter angle for two-photon subtracted non-gaussian states at $\gamma = 0.5$. Analog results hold for two-photon-added states.

Figure 5 shows numerical evidence that such relationship exists, since the more entangled states coincide exactly with those with higher extractable signal-to-noise ratios. This correlation would also explain why there exists no dependence of SNR_{extr} on the other passive optics operation, namely the phase shifter, not even when more than one single-photon operations are executed: PS is a transformation which introduces a phase on one of the quadratures with respect to the other, but always in a *local* sense, i.e. within each mode independently; as opposed to BS, which is a mode-mixing (and thus entangling) transformation.

Finally, we generalize the above results to higher number of modes. In this case, the

plotted values are the result of a free optimization over all parameters in the Gaussian set: N squeezing variables, $\frac{N(N-1)}{2}$ beam splitter angles, and N phase shifts. The absence of intersection in the curves shown in Fig.6 accounts for the fact that the hierarchy in extractable signal-to-noise ratios established by the stellar rank in the two-mode case is a property that can be generalized to larger N, and the existent increasing trend of SNR_{extr} with N suggests that bigger and more complex non-gaussian battery systems hold a promising potential as highly precise energy storage devices.

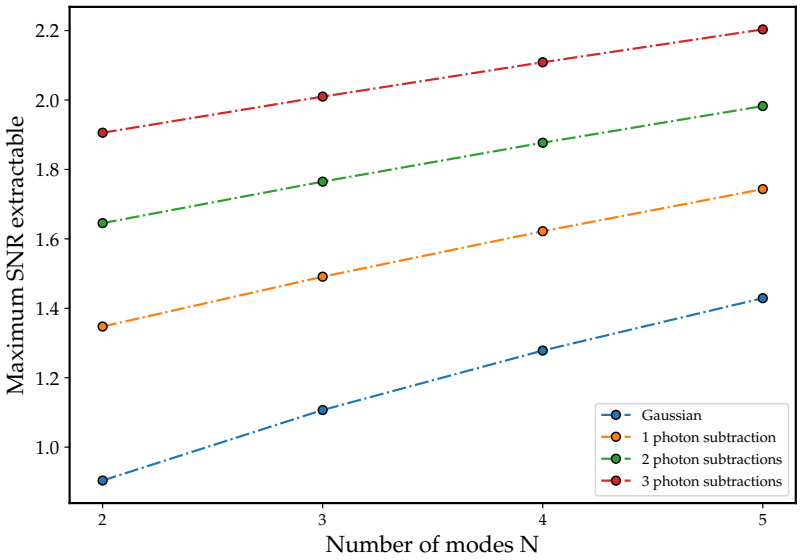

Figure 6: Scaling of maximum SNR_{extr} with number of modes, for different amounts of non-gaussian operations

The next chapter focuses on a second proposal for the application of our CV QONN. The same structure that we have employed for energy charging optimization is now utilized to address the simulation of Quantum Field Theory models. Light fields are systems with infinite-dimensional Hilbert spaces that abide by the bosonic statistics, which, as we will shortly argue, makes the CV framework a particularly natural choice for their description.

3 Simulation of lattice field theories

3.1 Motivation

The Standard Model of particle physics, which describes the electromagnetic, weak and strong nuclear forces, and which has so far demonstrated impressive success in making experimental predictions, is formulated within the framework of Quantum Field Theory. It inherits the description of particles as excitations of the underlying fields, the Lagrangian formalism, the central concept of gauge symmetry, and techniques such as renormalization and Feynmann diagrams [PS19]. This poses great importance on QFT as an indispensable tool in the comprehension of the fundamental interactions in nature. Moreover, QFT bridges different areas of physics by providing methods for solving complex problems ranging from high-energy to condensed matter physics [Wil75] [GQW74], or even aspects in quantum information theory [Kit03], with the systematic calculation of scattering amplitudes or the study of critical phenomena in statistical mechanics as some relevant examples.

Although much of the physics in the Standard Model is well understood and investigated through analytical perturbation theory, certain phenomena, such as confinement and chiral symmetry breaking, demand the application of non-perturbative methods[PS19]. The most commonly used technique to allow for numerical simulations and to cure divergences naturally present in the model is lattice regularization, which involves discretizing space-time into a grid and restricting the system to a finite volume [Rot11]. Lattice Gauge Theory, which emerges from this approach, is essential e.g. in Quantum Chromodynamics (QCD) because strong nuclear interactions cannot be treated as small perturbations [Wil74] in the low energy regime. Simulating gauge theories on a lattice not only rigorously tests various quantum field theories but also serves as a benchmark for theoretical predictions, helping to verify the consistency and accuracy of different models [MM94]. The connection with experimental realizations is achieved by taking the infinite volume and continuum (zero lattice spacing) limits [Cre84].

Current numerical simulations of gauge theories are unavoidably limited by the inherent difficulty faced by classical computers when reproducing quantum properties. On top of this, the so-called *sign problem* in the context of LGT limits the applicability of Monte Carlo methods, which are the state-of-the-art technique for the study of certain quantum systems, especially those with strong interactions where phase factors experience wide fluctuations. Other situations, like the study of dense nuclear matter, entail a sufficient increase in the complexity of the Lagrangian density as to turn Montecarlo simulations unfeasible. For these reasons, implementing QFT on quantum computers stands out as one of the most promising applications towards achieving significant quantum advantage. Some preliminary successful demonstrations in 1D gauge theories have already been achieved [MMS+16], but the leap to higher spatial dimensions appears to be extremely challenging, since the models become increasingly complex. Consequently, moving to simulations in 2D represents a major opportunity to tackle questions that are over the scope of classical devices.

The first step in this direction is to find a suitable Hamiltonian representation and encoding of the theory we seek to simulate. In particular, $U(k)$ Yang-Mills theory has so far mainly been reproduced relying on the traditional Hamiltonian formulation developed by Kogut and Susskind (KS) [KS75]. However, another possible Hamiltonian formulation can be derived from the lattice Yang-Mills action through the Orbifold construction intro-

duced by Kaplan, Katz, and Unsal in 2002 [KKU03]. This proposal was originally intended for the representation of supersymmetric theories, where it shows by construction a clear advantage over traditional lattice regularizations. However, even for non-supersymmetric theories, there is a motivation for studying Orbifold lattices when it comes to real-time quantum simulations, due to the simplicity of its Hamiltonian formulation. In the following section, we give an insight on this alternative Orbifold approach, in an attempt to compare it with the well-studied Kogut Susskind one, evaluate its performance at revealing the different phenomena and study its advantages and limitations.

3.2 Orbifold construction of U(1) lattice field theory

We will focus on pure gauge $U(1)$ Yang-Mills theory in $(2+1)$ space-time dimensions. The restriction to the symmetry group $U(1)$ makes our system serve as a simplified model for understanding the basic principles of gauge field theories before generalizing to more complex non-abelian gauge groups, and is also directly applicable to Quantum Electrodynamics (QED), whose gauge symmetry is precisely $U(1)$.

We introduce labels $\quad \vec{n} = (n_x, n_y) \quad n_i = 1, 2 \dots L$ for each of the points in our two-dimensional lattice of size $L \times L$. $x_{\vec{n}}, y_{\vec{n}}$ represent the complex dynamical variables that live on the links connecting $\vec{n}$ and $\vec{n} + \hat{x}, \vec{n} + \hat{y}$, which are associated to the spatial field components of the theory. The temporal component of the gauge field is denoted by $A_{\vec{n}}$, and will be set to zero for all lattice sites upon gauge fixing.

A local $U(k)$ gauge transformation at site $\vec{n}$ parametrised by $\Omega_{\vec{n}}$ is given by:

$$\vec{x}_{\vec{n}} \to \Omega_{\vec{n}} x_{\vec{n}} \Omega^{-1}_{\vec{n}+\hat{x}} \quad \vec{y}_{\vec{n}} \to \Omega_{\vec{n}} y_{\vec{n}} \Omega^{-1}_{\vec{n}+\hat{y}}$$
$$A_{\vec{n}} \longrightarrow \Omega_{\vec{n}} A_{\vec{n}} \Omega^{-1}_{\vec{n}} + \frac{i}{g_{1d}} \Omega_{\vec{n}} \partial_t \Omega^{-1}_{\vec{n}}$$

The gauge-invariant parametrization of variables in the Orbifold formulation reads:

$$x = \frac{1}{\sqrt{2} a g_{1d}} e^{a^{5/2} g_{1d} s_1} e^{i a^{5/2} g_{1d} A_1}$$
$$y = \frac{1}{\sqrt{2} a g_{1d}} e^{a^{5/2} g_{1d} s_2} e^{i a^{5/2} g_{1d} A_2}$$

In the limit of infinite scalar mass $m \to \infty$, that is, when the scalar fields decouple, s_1, s_2 are frozen to zero and hence we have that our variables x, y are the same as the unitary link variables U_x, U_y appearing in the Kogut-Susskind formulation up to a constant factor $\frac{1}{\sqrt{2} a g_{1d}}$. The dimensionless parameter g_{1d} is the Yang-Mills coupling constant, defining the interaction strength between the gauge fields. In the Orbifold lattice and other formulations of Yang-Mills theory, quantities are often computed as a function of $\frac{1}{g^2}$, a convention that arises naturally from perturbative expansions in the classical limit of the theory, corresponding to weak coupling $g \to 0$, where the fields are strongly suppressed and the quantum fluctuations become negligible. The generalization of this coupling constant to n space-time dimensions depends on the lattice spacing a through the relation: $g^2_{nd} = a^{n-1} g^2_{1d}$

The expression for the Hamiltonian is given in terms of the link variables x, y and their canonical conjugates p_x, p_y [BHRS24]:

$$\hat{H}_{orb} = \sum_{\vec{n}} T_r \Bigg[\underbrace{|p_{x,\vec{n}}|^2 + |p_{y,\vec{n}}|^2}_{\hat{H}_{kin}} + \underbrace{\frac{g_{1d}^2}{2} \left| x_{\vec{n}} x_{\vec{n}}^\dagger - x_{\vec{n}-\hat{x}}^\dagger x_{\vec{n}-\hat{x}} + y_{\vec{n}} y_{\vec{n}}^\dagger - y_{\vec{n}-\hat{y}}^\dagger y_{\vec{n}-\hat{y}} \right|^2}_{\hat{H}_{el}} \tag{19}$$

$$\underbrace{2g_{1d}^2 |x_{\vec{n}} y_{\vec{n}+\hat{x}} - y_{\vec{n}} x_{\vec{n}+\hat{y}}|^2}_{\hat{H}_B} \Bigg] + \Delta\hat{H}$$

$$\text{where} \quad \Delta\hat{H} = \frac{\mu^2 g_{4d}^2}{2a} \sum_{\vec{n}} \mathrm{Tr} \left(\left| x_{\vec{n}} x_{\vec{n}}^\dagger - \frac{1}{2a^2 g_{1d}^2} \right|^2 + \left| y_{\vec{n}} y_{\vec{n}}^\dagger - \frac{1}{2a^2 g_{1d}^2} \right|^2 \right) \tag{20}$$

is a scalar mass term added as a correction so that our lattice regularization satisfies the necessary condition that $x_{\vec{n}} x_{\vec{n}}^\dagger \simeq \frac{a}{2g_{4d}^2} \mathbb{1}_N$, $y_{\vec{n}} y_{\vec{n}}^\dagger \simeq \frac{a}{2g_{4d}^2} \mathbb{1}_N \quad \forall \vec{n}$

The commutation relations are (where $\hat{z}_\mu$ stands for the generalized spatial coordinate operator, $\mu, \nu = 1$ for $\hat{x}$, 2 for $\hat{y}$):

$$\left[\hat{z}_{\mu\vec{n}}, \hat{p}_{\nu\vec{n}'}^\dagger \right] = i\delta_{\mu\nu}\delta_{\vec{n}\vec{n}'}$$
$$[\hat{z}, \hat{p}] = \left[\hat{z}^\dagger, \hat{p}^\dagger \right] = [\hat{z}, \hat{z}] = [\hat{p}, \hat{p}] = \left[\hat{z}^\dagger, \hat{z}^\dagger \right] = \left[\hat{p}^\dagger, \hat{p}^\dagger \right] = 0$$

Each complex link variable can be decomposed in its real and imaginary parts, yielding two new independent, self-adjoint variables: $\hat{z} = \frac{\hat{z}^{(R)} + i\hat{z}^{(I)}}{\sqrt{2}}$, (and analogous for the conjugate momenta) with the following non-vanishing commutation relations:

$$\left[\hat{z}_{\mu\vec{n}}^{(R)}, \hat{p}_{\nu\vec{n}'}^{(R)} \right] = i\delta_{\mu\nu}\delta_{\vec{n}\vec{n}'} \qquad \left[\hat{z}_{\mu\vec{n}}^{(I)}, \hat{p}_{\nu\vec{n}'}^{(I)} \right] = i\delta_{\mu\nu}\delta_{\vec{n}\vec{n}'} \tag{21}$$

The generator of a local $U(1)$ transformation at site $\vec{n}$ is:

$$\hat{G}_{\vec{n}} = i \sum_{\mu=1}^{2} (-\hat{z}_{\mu,\vec{n}} \hat{p}_{\mu\vec{n}}^\dagger + \hat{p}_{\mu,\vec{n}} \hat{z}_{\mu,\vec{n}}^\dagger - \hat{z}_{\mu,\vec{n}-\mu}^\dagger \hat{p}_{\mu,\vec{n}-\mu} + \hat{p}_{\mu,\vec{n}-\mu}^\dagger \hat{z}_{\mu,\vec{n}-\mu}) \tag{22}$$

Due to the fact that the Hamiltonian is invariant under local $U(1)$ transformations, $[\hat{G}_{\vec{n}}, H] = 0$, Gauss' law constraint derives from this group generator and imposes that for any physical state, the expectation value of the operator $\hat{G}_{\vec{n}}$ vanishes at all lattice sites $\vec{n}$.

$$\hat{G}_{\vec{n}} |\text{phys}\rangle = 0 \tag{23}$$

It is important to note that in lattice field theory, the gauge fields, which are defined on the links between neighboring lattice points, are continuous functions $A_\mu(x)$ of space-time coordinates x. However, most quantum simulations of QFT use qubits or qudits, which are inherently discrete systems. This implies truncating the Hilbert space to a finite dimension by discretizing the range of possible field values. In [BGH+21] a truncation in the Fock basis is proposed, while the advantages of truncating in the coordinate basis are analysed in [BHRS24]. Either way implies a loss of accuracy in the simulation of the fields as the

cutoff becomes more restrictive.

In contrast with this, one can find a very natural mapping between the gauge degrees of freedom and those of continuous variable systems, making the latter more suitable simulators for LGT. In CV, the quadrature operators of a bosonic mode, which span continuous ranges of values, can be used to represent the field at each lattice point, taking advantage of the fact that field operators in QFT behave the same way (i.e. satisfy analogous commutation relations, see Eq.21) as bosonic position and conjugate momentum.

For this reason, the ultimate goal and current efforts in this project are being put towards removing the above-mentioned dimension cutoff, mandatory in discrete implementations, by embedding this theory into our CV QNN architecture. The Orbifold Hamiltonian reformulates the problem of simulating Yang-Mills theory and translates it into the simulation of a collection of coupled harmonic oscillators, allowing for the expression of position and momentum of each of them in terms of ladder operators applied to the different modes. With this, the admissibility condition on the observables of the theory to be cost functions of our neural network is directly fulfilled, making the Orbifold representation an ideal fit for our purposes. What we present in the results section below is a yet preliminary study of the one-plaquette system through exact diagonalisation of the Orbifold Hamiltonian, with Hilbert space truncation in the Fock basis with dimension $\Lambda = 3$ for each independent oscillator (i.e. with a maximum of two excited levels).

3.3 Results

For simplicity, we consider one single plaquette with four sites on its vertices without matter fields. This accounts for eight link variables representing the interacting gauge fields, considering real and imaginary parts separately. Each of these variables is treated as a quantum 3-level oscillator, so the dimension of the composite Hilbert space of the system is $|\mathcal{H}| = 3^8$. The Hamiltonian defining the dynamics of the plaquette is just obtained through the restriction of Eq. 19 to sites $\vec{n} \in \{(0,0),(0,1),(1,0),(1,1)\}$.

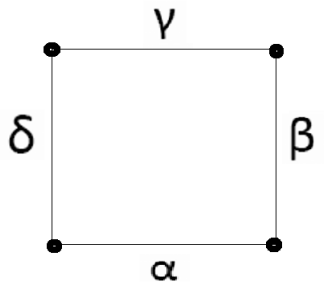

Figure 7: One plaquette lattice

The first quantities we are interested in obtaining are the ground state energy of the plaquette, together with the contribution to this energy of each of the four terms in the Hamiltonian. These values are plotted in Figures 8 and 9 with respect to the inverse of the squared coupling constant $\frac{1}{g^2}$, as mentioned above. The numerical values of the parameters applied to the figures are lattice spacing $a = 1$ and scalar mass $\mu = 1$.

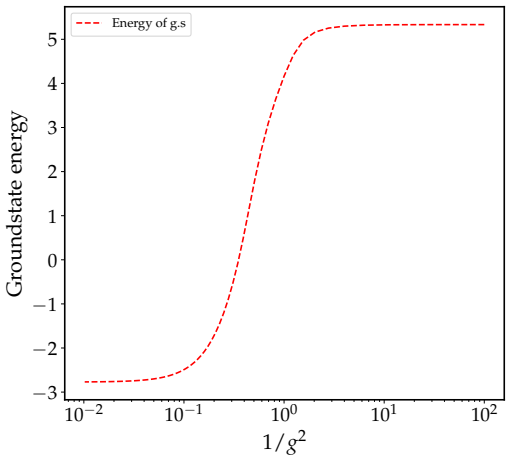

Figure 8: G.s of $\hat{H}$ via exact diagonalisation

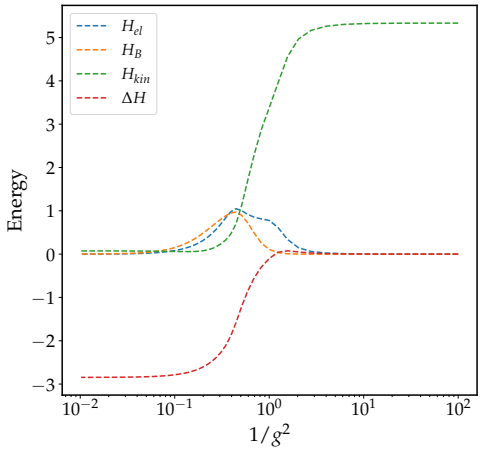

Figure 9: Contributions of $\hat{H}$ terms to g.s energy

An important sanity check worth making is that Gauss' law is fulfilled. This condition can be used to lower the requirements of a quantum simulation: in the Hamiltonian formulation of a gauge theory, only a very small subspace of $\mathcal{H}$ consists of gauge-invariant states. By applying Gauss' law, it is possible to eliminate some of the gauge fields (thus yielding an effective Hamiltonian with a lower amount of degrees of freedom) and obtain a formulation directly constrained to the gauge-invariant subspace. This results in a more resource-efficient encoding but also implies the appearance of long-range many-body interactions in the effective Hamiltonian which may lead to harder computational and implementation-related challenges. In our case, it has been sufficient to compute the expectation value of the four Gauss operators (associated to the four sites of the plaquette) on the obtained groundstate of $\hat{H}$ as a function of the coupling parameter, in order to conclude that Gauss law is satisfied so that all of our states of interest are physical.

We have also performed separate diagonalization of all the four terms $\hat{H}_{el}$, $\hat{H}_B$, $\hat{H}_{kin}$, $\Delta\hat{H}$ independently, and then computed the overlap between the resulting individual groundstates and those of the full Hamiltonian (see Fig.10).

We observe there is a clear regime separation at the intersection of the kinetic and electric curves, corresponding to $\frac{1}{g^2} \approx 0.7$. At this same point, there is also an interesting peak in the scalar mass corrections $\Delta\hat{H}$ curve, meaning that a phase transition is likely to be taking place around those coupling values. This transition comes, in addition, with a decrease in the energetic gap between the ground and first excited state, as can be observed in Figure 11. In contrast to what occurs in the Kogut-Susskind formulation, where the electric basis is used at small values of $\frac{1}{g^2}$, here the electric term's eigenstates coincide with those of the full Hamiltonian for small couplings, while in the $\frac{1}{g^2} < 1$ region the ground states are superpositions of many different elements of the electric basis.

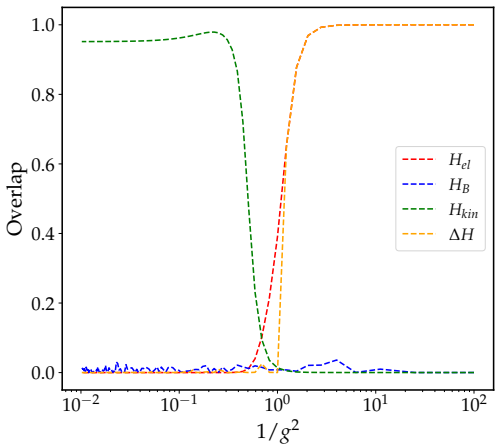

Figure 10: Overlaps between groundstates of full $\hat{H}$ and those of individual Hamiltonian terms

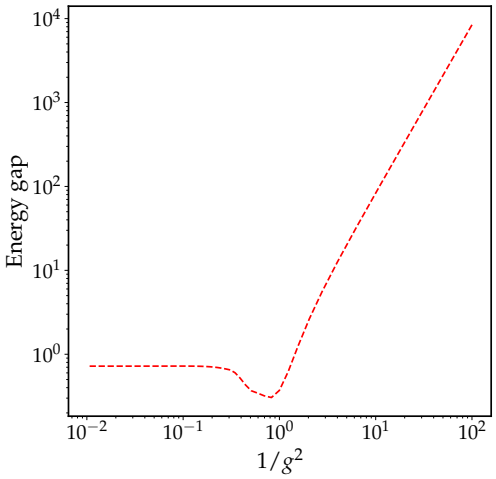

Figure 11: Mass gap of the Orbifold Hamiltonian

Lastly, we are interested in identifying an order parameter for the above-mentioned transition. In the context of lattice gauge theory, Wilson loops are the ones to play this role. A Wilson loop is a gauge-invariant observable constructed from the gauge field along a closed loop in space-time. Due to its local nature, it can be simulated on small lattices, such as the one we are considering. A particular example of Wilson loop, namely the plaquette operator:

$$\hat{\square} = \frac{1}{2N} \sum_{n=1}^{N} \left(\hat{x}_\alpha^\dagger \hat{y}_\beta^\dagger \hat{y}_\delta \hat{x}_\gamma + \hat{x}_\alpha \hat{y}_\beta \hat{y}_\delta^\dagger \hat{x}_\gamma^\dagger \right)_n \qquad N = \text{number of plaquettes}$$

which in the Kogut-Susskind representation has the same form as the magnetic field term in the Hamiltonian, allows for the identification of a transition between confinement and deconfinement regimes as its expectation value on the groundstates changes sign. In the Orbifold Hamiltonian there is a significant shift between the plaquette operator and the magnetic field term, as shown in Fig.12, and neither of them seems to be the adequate quantity to consider as order parameter, because although displaying a local minima in the seemingly interesting region, their values remain negative for all coupling strengths.

In Figure 13 the bipartite entanglement entropy of the ground state with respect to the bipartition of the system in half is plotted as a function of the coupling constant. We observe that in the two extremes the ground states are approximately product states, while correlations experience a rapid growth as the critical point is approached.

All the above results converge at pointing out a characteristic signature of three different phases, with a central one of stronger correlations close to the regime of unit coupling. Given these preliminary findings, it would be interesting to test our results on larger systems of N plaquettes, perhaps making use of tensor networks in order to make simulations computationally manageable. Exploring the effect of the truncation by gradually increasing the cutoff, and extrapolating our results to predict the behavior as the cutoff approaches infinity is also left for future work, together with the implementation of our continuous-variable QONN for infinite-dimensional, truncationless simulations of the Orbifold model,

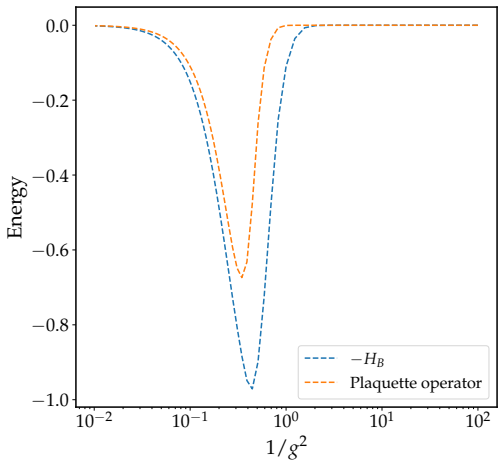

Figure 12: Expectation values of the magnetic Hamiltonian term (with opposite sign) and the plaquette operator on the groundstates of the system

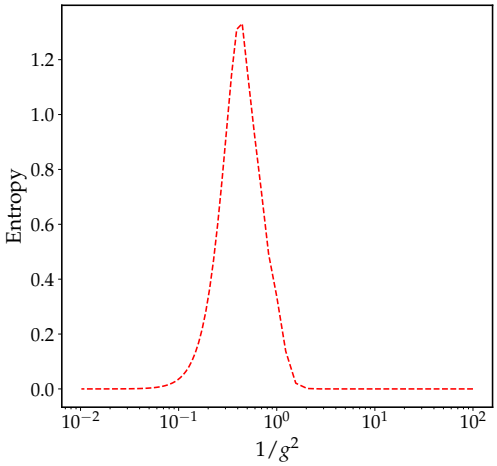

Figure 13: Bipartite entanglement entropy of groundstate with respect to the bipartition of modes (1,2,3,4)-(5,6,7,8)

which could potentially give us deeper insights on how this formulation compares to its alternatives and how accurately it resembles the underlying theory.

4 Conclusions and outlook

Throughout this thesis we have explored the potential of photonic circuits as simulation platforms for systems with infinite-dimensional degrees of freedom, by adopting a particular encoding of information in the continuous-valued quadrature observables. We have studied the components of a variational algorithm that naturally embeds features from quantum optics into classical optimization processes, and analysed both the experimental and mathematical construction of the most general Gaussian state, through parametrized squeezing and passive optics operations. Finally, upon introduction of non-gaussianity by means of iterative single-photon subtractions and additions, we have accessed a whole broader realm at which genuine non-classical properties can be observed and exploited for quantum information processing matters.

Our results regarding the evaluation of quantum batteries in terms of energy charging precision have shown not only that non-gaussian distributions outperform Gaussian ones, but also that within the former, there exists a hierarchy by which states with higher stellar ranks realize signal-to-noise ratio bounds that are not attainable for lower stellar rank states. Moreover, we have demonstrated that for non-gaussianity degrees above two single-photon operations, unitary charging through passive optics constitutes a source of precision enhancement and can be related to the generation of bipartite entanglement within battery systems. Lastly, the potential gain that could be obtained by scaling these energy storage devices to higher number of optical modes has also been outlined in this work.

With respect to the simulation of gauge theories, we have investigated the Orbifold construction of $U(1)$ Yang-Mills theory, which emerges as a more formally straightforward formulation than the traditional approach, encompassing features that make it particularly

suited to our variational architecture. We have looked at several properties of the Orbifold Hamiltonian's groundstate, including its energy and the contribution to it of the different Hamiltonian terms, its bipartite entanglement, the expectation value of the so-called plaquette operator and the mass gap of the model. Our results, obtained by means of exact diagonalization in a truncated Hilbert space, allow for identification of different regimes as a function of the coupling strength even in a yet simple model of maximally reduced size as is the case of one single plaquette. The main conclusion distilled from these outcomes is that further investigation of the Orbifold representation involving larger systems and easing the truncation constraints by employing a continuous-variable framework has the potential to unveil interesting attributes of the theory and exploit the power of quantum simulations in a classically intractable domain.

A number of directions stem from this work as possible topics of future research. On the one hand, a primary focus is set on overcoming the current limitations of our quantum optical neural network proposal, turning it into a more expressive algorithm, able to solve complex optimization problems and applicable to a wide spectrum of quantum simulation tasks. One of our initial assumptions was that of zero-mean Gaussian distributions, which, despite being the usual approach in most applications within the CV framework, still entails some degree of information loss. Thus, considering a generalization that includes the first-moments vector could be of interest to our purposes. Regarding non-gaussianity, our current ansatz is restricted to states consisting of a single product of ladder operators applied to a Gaussian state, and the admitted objective Hamiltonians must also display this same structure of single products of $\hat{a}$ and $\hat{a}^\dagger$. Hence, a possible enhancement would consist in removing these constraints so that the NN allows for different Hamiltonians and more general non-gaussian transformations, taking into account a wider portion of the Hilbert space of possible states of the system. On top of this, the implementation of natural gradient descent as optimization method in place of the classical alternatives could also result in a significant upgrade, thereby taking advantage of the continuous-variable formulation of the problem. Lastly, the conducted work described here focuses on a one-layer circuit, first performing passive optics operations on the input Gaussian state, and then applying non-linearity through photon additions and subtractions. However, linear combinations of these operations can be implemented in optical setups by alternating Gaussian unitaries and non-gaussian ladder operators. It is then natural to think that more expressivity could be achieved by resembling these alternating blocks through a multi-layer version of the neural network.

Once all these refinements to the QONN architecture have been accomplished, the next step would be the aforementioned application of the algorithm to simulations of infinite dimensional Hilbert space systems, extending its scope from the Orbifold one-plaquette model to more complex Hamiltonians, appearing in Quantum Field Theory and beyond.

Bibliography

[ADR82] Alain Aspect, Jean Dalibard, and Gérard Roger. Experimental test of bell's inequalities using time-varying analyzers. *Phys. Rev. Lett.*, 49:1804–1807, Dec 1982.

[AGW12] Alán Aspuru-Guzik and Philip Walther. Photonic quantum simulators. *Nat. Phys.*, 8(4):285–291, April 2012.

[BFGS18] Stephen M. Barnett, Gergely Ferenczi, Claire R. Gilson, and Fiona C. Speirits.

Statistics of photon-subtracted and photon-added states. *Physical Review A*, 98(1), July 2018.

[BGH+21] Alexander J. Buser, Hrant Gharibyan, Masanori Hanada, Masazumi Honda, and Junyu Liu. Quantum simulation of gauge theory via orbifold lattice. *Journal of High Energy Physics*, 2021(9), September 2021.

[BHRS24] Georg Bergner, Masanori Hanada, Enrico Rinaldi, and Andreas Schafer. Toward qcd on quantum computer: Orbifold lattice approach, 2024.

[BJML10] Erwan Bimbard, Nitin Jain, Andrew MacRae, and A. I. Lvovsky. Quantum-optical state engineering up to the two-photon level. *Nature Photonics*, 4(4):243–247, February 2010.

[BM62] Claude Bloch and Albert Messiah. The canonical form of an antisymmetric tensor and its application to the theory of superconductivity. *Nuclear Physics*, 39:95–106, 1962.

[CC22] Gianfranco Cariolaro and Roberto Corvaja. Implementation of two-mode gaussian states whose covariance matrix has the standard form. *Symmetry*, 14(7), 2022.

[CFGM21] Ulysse Chabaud, Giulia Ferrini, Frédéric Grosshans, and Damian Markham. Classical simulation of gaussian quantum circuits with non-gaussian input states. *Phys. Rev. Res.*, 3:033018, Jul 2021.

[CGQ+23] Francesco Campaioli, Stefano Gherardini, James Q. Quach, Marco Polini, and Gian Marcello Andolina. Colloquium: Quantum batteries, 2023.

[CHK+20] Iacopo Carusotto, Andrew A. Houck, Alicia J. Kollár, Pedram Roushan, David I. Schuster, and Jonathan Simon. Photonic materials in circuit quantum electrodynamics. *Nature Physics*, 16(3):268–279, March 2020. Publisher Copyright: © 2020, Springer Nature Limited.

[CM22] Ulysse Chabaud and Saeed Mehraban. Holomorphic representation of quantum computations. *Quantum*, 6:831, October 2022.

[Cre84] M. Creutz. *Quarks, Gluons and Lattices*. Cambridge University Press, 1984.

[FCA+18] Dario Ferraro, Michele Campisi, Gian Marcello Andolina, Vittorio Pellegrini, and Marco Polini. High-power collective charging of a solid-state quantum battery. *Physical Review Letters*, 120(11), March 2018.

[Fey81] Richard P. Feynman. Simulating physics with computers, 1981. *International Journal of Theoretical Physics, vol. 21, no. 6/7*, 1981.

[FH18] Nicolai Friis and Marcus Huber. Precision and work fluctuations in gaussian battery charging. *Quantum*, 2:61, April 2018.

[GQW74] H. Georgi, H. R. Quinn, and S. Weinberg. Hierarchy of interactions in unified gauge theories. *Phys. Rev. Lett.*, 33:451–454, Aug 1974.

[HJ19] Tobias Hartung and Karl Jansen. Zeta-regularized vacuum expectation values. *J. Math. Phys.*, 60(9):093504, 2019.

[ISS18] L. ISSERLIS. On a formula for the product-moment coefficient of any order of a normal frequency distribution in any number of variables. *Biometrika*, 12(1-2):134–139, 11 1918.

[KBA+19] Nathan Killoran, Thomas R. Bromley, Juan Miguel Arrazola, Maria Schuld, Nicolás Quesada, and Seth Lloyd. Continuous-variable quantum neural networks. *Physical Review Research*, 1(3), October 2019.

[Kit03] A.Yu. Kitaev. Fault-tolerant quantum computation by anyons. *Annals of Physics*, 303(1):2–30, January 2003.

[KKU03] David B Kaplan, Emanuel Katz, and Mithat Unsal. Supersymmetry on a spatial lattice. *Journal of High Energy Physics*, 2003(05):037–037, May 2003.

[KS75] John Kogut and Leonard Susskind. Hamiltonian formulation of wilson's lattice gauge theories. *Phys. Rev. D*, 11, 01 1975.

[MLA+22] Lars S Madsen, Fabian Laudenbach, Mohsen Falamarzi Askarani, Fabien Rortais, Trevor Vincent, Jacob F F Bulmer, Filippo M Miatto, Leonhard Neuhaus, Lukas G Helt, Matthew J Collins, Adriana E Lita, Thomas Gerrits, Sae Woo Nam, Varun D Vaidya, Matteo Menotti, Ish Dhand, Zachary Vernon, Nicolás Quesada, and Jonathan Lavoie. Quantum computational advantage with a programmable photonic processor. *Nature*, 606(7912):75–81, June 2022.

[MM94] I. Montvay and G. Münster. *Quantum Fields on a Lattice*. Cambridge University Press, 1994.

[MMS+16] Esteban A. Martinez, Christine A. Muschik, Philipp Schindler, Daniel Nigg, Alexander Erhard, Markus Heyl, Philipp Hauke, Marcello Dalmonte, Thomas Monz, Peter Zoller, and Rainer Blatt. Real-time dynamics of lattice gauge theories with a few-qubit quantum computer. *Nature*, 534(7608):516–519, June 2016.

[NNNH+06] J. S. Neergaard-Nielsen, B. Melholt Nielsen, C. Hettich, K. Mølmer, and E. S. Polzik. Generation of a superposition of odd photon number states for quantum information networks. *Phys. Rev. Lett.*, 97:083604, Aug 2006.

[OFV09] Jeremy L. O'Brien, Akira Furusawa, and Jelena Vučković. Photonic quantum technologies. *Nature Photonics*, 3(12):687–695, December 2009.

[PS19] Michael E Peskin and Daniel V Schroeder. *An introduction to quantum field theory*. CRC Press, London, England, September 2019.

[Rot11] Heinz J Rothe. *Lattice Gauge Theories: An Introduction*. WORLD SCIENTIFIC, November 2011.

[SAC+24] Paolo Stornati, Antonio Acin, Ulysse Chabaud, Alexandre Dauphin, Valentina Parigi, and Federico Centrone. Variational quantum simulation using non-gaussian continuous-variable systems, 2024.

[Ser21] Alessio Serafini. *Quantum continuous variables*. CRC Press, London, England, December 2021.

[SOEC18] Gregory R. Steinbrecher, Jonathan P. Olson, Dirk Englund, and Jacques Carolan. Quantum optical neural networks, 2018.

[SV05] E. Shchukin and W. Vogel. Inseparability criteria for continuous bipartite quantum states. *Phys. Rev. Lett.*, 95:230502, Nov 2005.

[TR19] Si-Hui Tan and Peter P. Rohde. The resurgence of the linear optics quantum interferometer — recent advances applications. *Reviews in Physics*, 4:100030, 2019.

[Wic50] G. C. Wick. The evaluation of the collision matrix. *Phys. Rev.*, 80:268–272, Oct 1950.

[Wil36] Jack Williamson. On the algebraic problem concerning the normal forms of linear dynamical systems. *American Journal of Mathematics*, 58:141, 1936.

[Wil74] K. G. Wilson. Confinement of quarks. *Phys. Rev. D*, 10:2445–2459, 1974.

[Wil75] Kenneth G. Wilson. The renormalization group: Critical phenomena and the kondo problem. *Rev. Mod. Phys.*, 47:773–840, Oct 1975.

[ZWD+20] Han-Sen Zhong, Hui Wang, Yu-Hao Deng, Ming-Cheng Chen, Li-Chao Peng, Yi-Han Luo, Jian Qin, Dian Wu, Xing Ding, Yi Hu, Peng Hu, Xiao-Yan Yang, Wei-Jun Zhang, Hao Li, Yuxuan Li, Xiao Jiang, Lin Gan, Guangwen Yang, Lixing You, Zhen Wang, Li Li, Nai-Le Liu, Chao-Yang Lu, and

Jian-Wei Pan. Quantum computational advantage using photons. *Science*, 370(6523):1460–1463, December 2020.

A Calculation of expectation values on non-gaussian states

The procedure for computing the cost function in our variational algorithm picks up the assumption that the observable of interest can be written as a product of ladder operators, and also that the output state after the whole gate set can be written as another product of ladder operators acting on an underlying Gaussian state with density matrix $\hat{\rho}_G$:

$$\hat{M} = \Pi_j \hat{a}_j^{\#}, \quad \hat{\rho}_{NG} = \frac{1}{K} \Pi_i \hat{a}_i^{\#} \hat{\rho}_G (\hat{a}_i^{\#})^\dagger$$

where $\# \in \{\dagger, \cdot\}$ denotes the type of ladder operator (creation or annihilation, respectively), and $K := \mathrm{Tr}\left[\Pi_i \hat{a}_i^{\#} \rho_G (\hat{a}_i^{\#})^\dagger\right]$ is a normalization factor that comes from the fact that ladder operators are non-unitary, whose numerical value can be obtained through the exact same method that we are describing. By the cyclic property of the trace:

$$\mathrm{Tr}\left[\hat{M}\hat{\rho}_{NG}\right] = \frac{1}{K} \mathrm{Tr}\left[\hat{a}_{S_n}^\dagger \dots \hat{a}_{S_1}^\dagger \hat{a}_{C_m}^\dagger \dots \hat{a}_{C_1}^\dagger \hat{a}_{C_1} \dots \hat{a}_{C_m} \hat{a}_{S_1} \dots \hat{a}_{S_n} \hat{\rho}_G\right]$$

where operators with subscript S_i are those implementing the photon subtractions (analogous for additions by taking hermitian conjugates) on mode i of the Gaussian state, and those with subscript C_j comprise the expression of the observable $\hat{M}$ whose expectation value we wish to calculate. From Wick's theorem [Wic50] we know that the expectation value of a single product of ladder operators can be decomposed as the following sum:

$$\mathrm{Tr}\left[\hat{a}_{S_n}^\dagger \dots \hat{a}_{S_1}^\dagger \hat{a}_{C_m}^\dagger \dots \hat{a}_{C_1}^\dagger \hat{a}_{C_1} \dots \hat{a}_{C_m} \hat{a}_{S_1} \dots \hat{a}_{S_n} \hat{\rho}_G\right] = \sum_{\mathcal{P}} \prod_{\{(p_1,\#),(p_2,\#)\}\in\mathcal{P}} \mathrm{Tr}\left[\hat{a}_{p_1}^{\#} \hat{a}_{p_2}^{\#} \hat{\rho}_G\right],$$

where $\mathcal{P}$ is the set of all possible perfect matchings of the $2n + m$ indices $(p_k, \#) \in \{C_1, \dots, C_m, S_1, \dots, S_n\} \times \{\dagger, \cdot\}$ of the ladder operators. It is worth noting that the grouping of the operators in pairs is possible due to the fact that for an initial Gaussian state with no displacement, all the odd order correlations vanish, thus if we had an odd number of $\hat{a}^{\#}$ in the product, the expectation value would trivially be zero. All we are left with are expectation values of pairs of annihilation or creation operators on a Gaussian state, which can be computed by using the following identities:

$$\begin{aligned}
I_1 &= \mathrm{Tr}\left[\hat{a}_j^\dagger \hat{a}_k^\dagger \hat{\rho}_G\right] = \frac{1}{4}\left[V_{jk} - V_{j+N,k+N} - i\left(V_{j,k+N} + V_{j+N,k}\right)\right], \\
I_2 &= \mathrm{Tr}\left[\hat{a}_j \hat{a}_k \hat{\rho}_G\right] = I_1^* \\
I_3 &= \mathrm{Tr}\left[\hat{a}_j^\dagger \hat{a}_k \hat{\rho}_G\right] = \frac{1}{4}\left[V_{jk} + V_{j+N,k+N} + i\left(V_{j,k+N} - V_{j+N,k}\right) - 2\delta_{jk}\right], \\
I_4 &= \mathrm{Tr}\left[\hat{a}_j \hat{a}_k^\dagger \hat{\rho}_G\right] = \delta_{jk} + I_3^*
\end{aligned}$$

where V_{jk} is the (j, k) matrix element of the $2N \times 2N$ covariance matrix of the quadratures of the state $\hat{\rho}_G$. A pseudocode illustrating this approach for trace computation is shown below.

Algorithm 1 Expectation value of observable $\hat{M}$ on a non-gaussian state

$\sigma \leftarrow$ covariance matrix of ρ_G (array)
NonGaussOps $\leftarrow$ list of non-gaussian operations

▷ e.g [-1] for subtraction on mode 1

OpsM $\leftarrow$ list of ladder operators defining $\hat{M}$
ModesM $\leftarrow$ list of modes on which OpsM acts

▷ e.g for $\hat{M} = \hat{N}_1 = \hat{a}_1^\dagger \hat{a}_1$, OpsM=['adag','a'] and ModesM=[1,1]

FullString $\leftarrow$ JOIN(NonGaussOps, OpsM, ModesM)

▷ Joins ladder operators from $\hat{M}$ and ρ_{NG}, applying cyclic property of the trace

Matchings $\leftarrow$ PERFECT MATCHINGS(FullString)
Trace $\leftarrow 0$

for matching in Matchings **do**
    factor $\leftarrow 1$
    for item in matching **do**
        factor $\times =$ TRACE(item) ▷ TRACE implements the identities I_1, I_2, I_3, I_4
    Trace $+=$ factor

return Trace

B Critical temperature

In order to demonstrate that Fock states are not trivially optimal regardless of the system fluctuations, we consider the two-mode vacuum $|0\rangle$ state, to which we apply a squeezing operation, no passive optics, and one single-photon addition. After this circuit, for all values of z, the outcome will be a squeezed photon-added state, except for $z = 1$ (no squeezing), which will correspond to the Fock state $|1\rangle$. In Fig.14 we show a density plot in which SNR_{extr} is evaluated with respect to both z and noise of the system.

What we observe is that the Fock state, for low fluctuations γ (temperature close to zero), is indeed optimal. However, as temperature increases, the Fock state's ratios undergo a significant drop, up to a point where they are the worst in comparison to other CV states to which some squeezing has been applied. In contrast, highly-squeezed states are less sensible to the increase in noise level, and they display good signal-to-noise ratios independently of temperature. Analogous behaviours are obtained for more photon additions (i.e. for Fock states $|2\rangle$,$|3\rangle$, etc) although the switch in regimes (from optimal to suboptimal) takes place at different temperatures for each of them. Nonetheless, the simple existence of such a transition justifies our optimization purposes, since otherwise one could always state that Fock states were trivially the solution to the problem.

In Figure 14 we have also added a dashed curve along the points of the graph where $SNR_{extr} = 1$. This value is precisely the maximum ratio attainable by Gaussian states (in

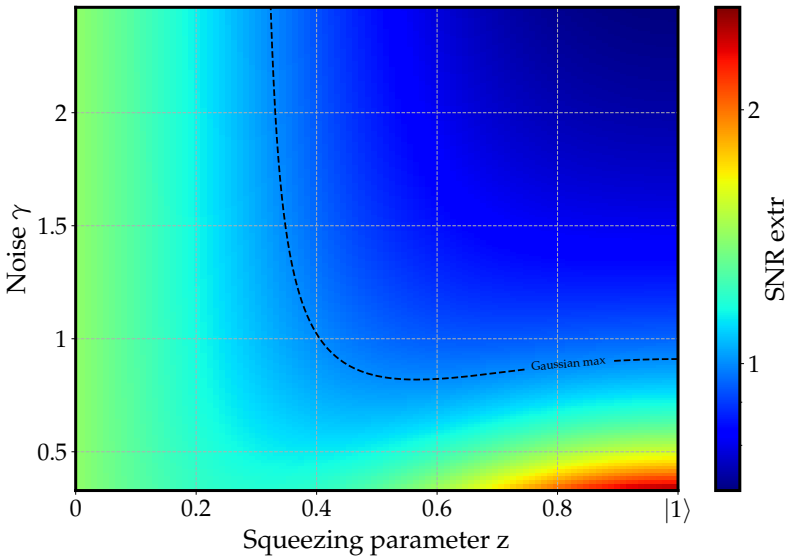

Figure 14: SNR_{extr} as a function of squeezing and noise. The limit $z = 1$ corresponds to the thermal Fock state $|1\rangle$

the limit of zero noise $\gamma = 0$) according to Figure 2 and Eq.17. This curve establishes a boundary between classical and quantum regimes, in the sense that one can find classically reproducible distributions that are better batteries than all states with $SNR_{extr} < 1$, while states on the bottom left have either sufficient squeezing or enough purity as to outperform all possible Gaussian states.

C Photon antibunching and signal-to-noise ratio

Different light sources give rise to different photon statistics (i.e. different distributions of the time intervals elapsed between successive photons). Three regimes can be distinguished among these distributions, according to whether the mean number of photons $\langle N \rangle$ within a time interval is smaller (super-Poissonian), equal (Poissonian) or greater (sub-Poissonian) than its variance $(\Delta N)^2$. Both Poissonian and super-Poissonian light can be described by a semi-classical theory, in which the light source is modeled as an electromagnetic wave, while sub-Poissonian statistics are indicative of strictly non-classical light.

Sub-Poissonian light sources are preferable in various applications because they exhibit lower photon-number fluctuations, which is advantageous in high-precision measurements and information processing tasks where minimization of the noise plays a significant role. Moreover, devices with well-defined photon statistics, such as single-photon emitters, are essential for quantum communication and quantum cryptography, since a controllable photon output in this context is critical for encoding and transmitting quantum information securely.

An equivalent definition for sub-Poissonian statistics is the presence of photon antibunching, a quantum optical phenomenon that implies that two photons are more likely to be detected independently than in pairs. Quantum states of light undergo this process

whenever the so-called second-order correlation function is smaller than unity:

$$g^{(2)} = \frac{\left\langle : \left(\sum_k \hat{a}_k^\dagger \hat{a}_k\right)^2 : \right\rangle}{\left\langle \sum_k \hat{a}_k^\dagger \hat{a}_k \right\rangle^2} < 1 \iff \text{antibunching} \tag{24}$$

The following derivations show that this quantum-optical parameter has a strong relationship with our figure of merit, namely the extractable signal-to-noise ratio, in terms of which the requirement for the antibunching phenomenon to take place can also be expressed. Calculations are performed for the two-mode case for the sake of simplicity.

$$\begin{aligned} g^{(2)} &= \frac{\left\langle : \left(a_1^\dagger a_1 + a_2^\dagger a_2\right)^2 : \right\rangle}{\left\langle a_1^\dagger a_1 + a_2^\dagger a_2 \right\rangle^2} = \frac{\left\langle : a_1^\dagger a_1 a_1^\dagger a_1 + 2 a_1^\dagger a_1 a_2^\dagger a_2 + a_2^\dagger a_2 a_2^\dagger a_2 : \right\rangle}{\left\langle a_1^\dagger a_1 + a_2^\dagger a_2 \right\rangle^2} = \\ &= \frac{\left\langle a_1^{\dagger 2} a_1^2 \right\rangle + 2\left\langle a_1^\dagger a_2^\dagger a_1 a_2 \right\rangle + \left\langle a_2^{\dagger 2} a_2^2 \right\rangle}{\left\langle a_1^\dagger a_1 + a_2^\dagger a_2 \right\rangle^2} = \frac{\left\langle a_1^{\dagger 2} a_1^2 \right\rangle + 2\left\langle a_1^\dagger a_2^\dagger a_1 a_2 \right\rangle + \left\langle a_2^{\dagger 2} a_2^2 \right\rangle}{\langle N \rangle^2} \end{aligned} \tag{25}$$

and since

$$\begin{aligned} &(\Delta N)^2 = \langle N^2 \rangle - \langle N \rangle^2 = \left\langle \left(a_1^\dagger a_1 + a_2^\dagger a_2\right)^2 \right\rangle - \left(\left\langle a_1^\dagger a_1 \right\rangle + \left\langle a_2^\dagger a_2 \right\rangle\right)^2 \\ &= \left\langle a_1^\dagger a_1 a_1^\dagger a_1 \right\rangle + 2\left\langle a_1^\dagger a_1 a_2^\dagger a_2 \right\rangle + \left\langle a_2^\dagger a_2 a_2^\dagger a_2 \right\rangle - \left(\left\langle a_1^\dagger a_1 \right\rangle + \left\langle a_2^\dagger a_2 \right\rangle\right)^2 \\ &= \left\langle a_1^{\dagger 2} a_1^2 \right\rangle + \langle a_1^\dagger a_1 \rangle + 2\left\langle a_1^\dagger a_2^\dagger a_1 a_2 \right\rangle + \left\langle a_2^{\dagger 2} a_2^2 \right\rangle + \langle a_2^\dagger a_2 \rangle - \left(\left\langle a_1^+ a_1 \right\rangle + \left\langle a_2^\dagger a_2 \right\rangle\right)^2 \\ &= \left\langle a_1^{\dagger 2} a_1^2 \right\rangle + 2\left\langle a_1^\dagger a_2^\dagger a_1 a_2 \right\rangle + \left\langle a_2^{\dagger 2} a_2^2 \right\rangle + \langle N \rangle - \langle N \rangle^2 \end{aligned} \tag{26}$$

we arrive at

$$g^{(2)} = \frac{(\Delta N)^2 - \langle N \rangle + \langle N \rangle^2}{\langle N \rangle^2} = \frac{(\Delta N)^2}{\langle N \rangle^2} - \frac{1}{\langle N \rangle} + 1 \tag{27}$$

which, on account of Eq.14, relates to the extractable signal-to-noise ratio as:

$$SNR_{extr} = \frac{E - E_0}{\Delta E} = \frac{\langle N \rangle - N_0}{\Delta N} \implies g^{(2)} = \left(SNR_{extr} + \frac{N_0}{\Delta N}\right)^{-2} - \frac{1}{\langle N \rangle} + 1 \tag{28}$$

So the condition for photon antibunching established in Eq.24, only fulfilled by non-gaussian states, can equivalently be written in terms of our figure of merit through the following relation:

$$\left(SNR_{extr} + \frac{N_0}{\Delta N}\right)^2 > \langle N \rangle \iff \text{antibunching} \tag{29}$$

This inequality implies, since N_0 is a constant, that for a fixed average energy (or equivalently mean photon number $\langle N \rangle$), the process of antibunching will be favored by more precise batteries, which will display smaller ΔN (and consequently higher SNR_{extr}) so that the left-hand side of Eq.29 is more likely to outweigh the right-hand side.

D Experimental realization of non-gaussianity

Despite being mainly concerned about their mathematical representation, we found it useful to give a brief insight into how the single photon operations of subtraction and addition

are realized in state-of-the-art quantum hardware.

For photon subtraction, the input Gaussian state is sent through a weakly reflective beam splitter, which splits the incoming light into two modes: one that continues in the original path (transmitted mode) and one that is reflected. The latter is directed to a single-photon detector. When the detector clicks it indicates that a photon has been detected, so given that this condition occurs, the state of the transmitted mode is effectively a photon-subtracted state.

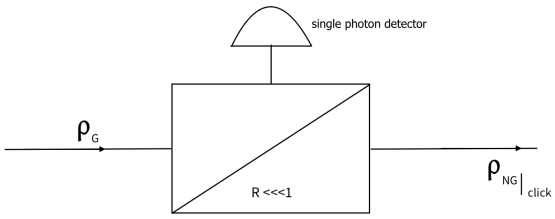

Figure 15: Conditional photon subtraction by means of a beam splitter and a photodetector.

Instead of fixing the reflectivity of the beam splitter, we could also consider it as a tunable parameter included in the optimization. Different values of this parameter would lead to potentially higher success probabilities of the photon-subtraction process (more frequent clicks), and at the same time to more general non-gaussian states, increasing the expressivity of the resulting neural network.

To add a photon to an incoming Gaussian state, a pump laser beam is directed onto a nonlinear crystal to produce pairs of photons (signal and idler) via spontaneous parametric down-conversion. The idler photon heralds the addition of a photon to the signal mode, in the sense that conditioned on its detection (that is, on the click of the photodetector), the state of the signal mode is a photon-added state.

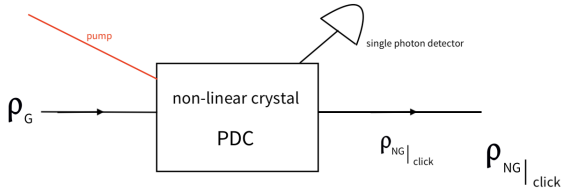

Figure 16: Conditional photon addition using a pump beam, a non-linear crystal, and a photodetector.

E Codes on Github

All the Python files and figures related to and appearing in this thesis can be found in the following repositories:

SNR for Gaussian batteries project
Orbifold formulation of LGT project